Taylor & Francis
Taylor & Francis Group

Canadian Metallurgical Quarterly
The Canadian Journal of Metallurgy and Materials Science

ISSN: (Print) (Online) Journal homepage: https://www.tandfonline.com/loi/ycmq20

Kinetics of cupric leaching of pyrite in 4 M NaCl solutions

Cinétique de la lixiviation cuivrique de la pyrite dans des solutions de NaCl 4M

Katherine Jaramillo & Tomás Vargas

To cite this article: Katherine Jaramillo & Tomás Vargas (2020) Kinetics of cupric leaching of pyrite in 4 M NaCl solutions, Canadian Metallurgical Quarterly, 59:3, 360-367, DOI: 10.1080/00084433.2020.1780559

To link to this article: https://doi.org/10.1080/00084433.2020.1780559

Published online: 22 Jun 2020.

CANADIAN METALLURGICAL QUARTERLY
2020, VOL. 59, NO. 3, 360–367
https://doi.org/10.1080/00084433.2020.1780559

RESEARCH ARTICLE

Kinetics of cupric leaching of pyrite in 4 M NaCl solutions
Cinétique de la lixiviation cuivrique de la pyrite dans des solutions de NaCl 4M

Katherine Jaramillo [a] and Tomás Vargas [b,c]

[a]Department of Mining Engineering, University of Chile, Santiago, Chile; [b]Department of Chemical Engineering, Biotechnology and Materials, University of Chile, Santiago, Chile; [c]Advanced Mining Technology Center (AMTC), University of Chile, Santiago, Chile

ABSTRACT

Cupric chloride leaching is an attractive alternative for the treatment of pyritic refractory gold ores. In this context, the kinetics of pyrite dissolution was studied in cupric chloride solutions containing 4 M NaCl. Pyrite leaching experiments were conducted in a stirred tank reactor for 250 h. The effect of temperature was evaluated at 45°C, 60°C and 75°C, while the effect of [Cu (II)] was evaluated with solutions containing 0.054, 0.252 and 0.512 M. The results showed that the increase in temperature and [Cu (II)] improved the rate of pyrite dissolution. The fraction of pyrite oxidised to sulphate ranged from 52% to 75%. Sulphate formation correlated well with the number of holes and cracks formed on leached pyrite particles. The kinetics of pyrite dissolution fitted well to the shrinking core model with chemical reaction control ($T \leq 60$°C and [Cu (II)] ≤ 0.054 M) or mixed control ($T > 60$°C and [Cu (II)] > 0.054 M). The activation energy was 73.102 kJ/mol and the dependence of [Cu (II)] was proportional to $[Cu(II)]^{0.230}$.

La lixiviation au chlorure cuivrique est une alternative attirante pour le traitement des minerais d'or réfractaires pyriteux. Dans ce contexte, on a étudié la cinétique de dissolution de la pyrite dans des solutions de chlorure cuivrique contenant du NaCl 4M. On a effectué des expériences de lixiviation de pyrite dans un réacteur à cuve agitée pendant 250 heures. On a évalué l'effet de la température à 45, 60 et 75°C alors que l'on a évalué l'effet du [Cu(II)] avec des solutions contenant 0.054, 0.252 et 0.512 M. Les résultats ont montré que l'augmentation de la température et du [Cu(II)] améliorait la vitesse de dissolution de la pyrite. La fraction de pyrite oxydée en sulfate variait de 52 à 75%. La formation de sulfate était bien corrélée avec le nombre de trous et de fissures formés sur les particules lixiviées de pyrite. La cinétique de dissolution de la pyrite correspondait bien au modèle du noyau rétrécissant avec contrôle de la réaction chimique ($T \leq 60$°C et [Cu (II)] ≤ 0.054 M) ou contrôle mixte ($T > 60$°C et [Cu (II)] > 0.054 M). L'énergie d'activation était de 73.102 kJ/mole et la dépendance de [Cu (II)] était proportionnelle à $[Cu\ (II)]^{0.230}$.

ARTICLE HISTORY
Received 26 July 2019
Accepted 5 June 2020

KEYWORDS
Refractory gold ores; pyrite leaching; cupric leaching; chloride leaching

1. Introduction

Pyrite (FeS_2) is the most abundant sulphide mineral on earth and in some cases, it may be found occluding precious metals such as gold and silver in its structure, the so-called refractory gold ores [1,2]. In these ores, an initial oxidative pretreatment is necessary in order to break down the pyritic matrix and improve the access of leaching reagents to the released valuable metal [3,4]. Conventionally, this is achieved by partial oxidation pretreatment of pyrite using roasting [5], pressure leaching [6] or bioleaching [7]. Gold is subsequently dissolved by a cyanidation stage in alkaline conditions [3,4].

Chloride leaching with Cu (II) is an attractive alternative to replace the previous approach, avoiding the use of cyanide and enabling to leach refractory gold ores in one single stage [8,9]. In chloride systems, the cupric ions act as an oxidising agent with a high oxidative potential which can dissolve sulphides [10–12] and simultaneously dissolve the gold as a chloride complex in a single stage process at atmospheric pressure [8,9]. Gold forms a stable complex with chloride such as $[AuCl_4]^-$ or $[AuCl_2]^-$ [8,13]. Furthermore, in chloride solutions, cupric ions may be continuously regenerated by the oxidation of the formed cuprous ions with oxygen, thus, oxygen acts as a final electron acceptor [11,12,14,15].

The behaviour of pyrite in chloride solutions with cupric ion has been studied but its kinetics and stoichiometry are not yet fully clarified. Some researchers have focused on the electrochemistry of pyrite in chloride solutions, reporting information on the anodic and cathodic behaviour of pyrite in chloride solutions with copper and iron ions [16–18]. Other authors proposed linear regression models to predict open circuit potential

CONTACT Tomás Vargas tvargas@ing.uchile.cl

and corrosion current density of pyrite in cupric chloride solutions [9,19] and conducted leaching tests with pyrite concentrate to validate these models [19]. However, there is not yet a study describing the kinetics of cupric leaching of pyrite in chloride solutions based on a phenomenological model.

In this work, we present a study of the kinetics of leaching of a particulate pyrite in cupric chloride solutions containing 4 M NaCl at different temperatures and different Cu (II) concentrations in order to establish the rate-determining step, to determine the kinetic parameters and to develop a mathematic expression of the pyrite dissolution according to the shrinking core model. Also, the stoichiometric reaction of the pyrite dissolution will be characterised.

2. Materials and methods

2.1. Material preparation and characterisation

The pyrite sample was prepared by grinding pyrite crystals in a porcelain mortar and electric mortar and separating by sieving the particles in the range −75 + 125 μm. Then, pyrite was cleaned to remove any remaining fine particles and to eliminate any oxides from the grain surfaces with acid treatment [20]. The pyrite sample was characterised by X-ray diffraction (XRD) and Scanning Electron Microscopy with Energy Dispersive X-ray spectrometer (SEM-EDX).

2.2. Leaching experiments

The apparatus used for leaching studies consisted of a 1.5 L glass reactor with a water jacket for temperature control. The lid had ports for inserting a glass tube for bubbling air into the reactor, three-bladed glass impeller mounted on a stirring shaft and a thermocouple. The stirring rate was maintained at 200 rev min^{-1} and an air pump was used to bubble air into the reactor at a flow of 0.06 L/s.

Leaching experiments were conducted with 10 g of pyrite sample in 1 L of leaching solution containing 4.0 M NaCl (Merck, 99.99% purity), 0.1 M HCl (Merck, 37% purity) and different concentrations of cupric ions added as $CuCl_2 \cdot 2H_2O$ (Merck, 99% purity). Air was continuously bubbled into the reactor during every experiment in order to regenerate cupric ions. The effect of temperature was evaluated in experiments at 45°C, 60°C and 75°C using a solution with 0.054 M Cu (II). The effect of Cu (II) was evaluated in experiments in solutions with 0.054, 0.252 and 0.512 M Cu (II) at 60°C. A summary of experimental conditions for each leaching experiment is shown in Table 1.

Table 1. Experimental temperature and Cu (II) concentration used in the pyrite leaching experiments.

Experiment	A	B	C	D	C
Temperature (°C)	45	60	75	60	60
$[Cu\ (II)]_o$ (mole/L)	0.054	0.054	0.054	0.252	0.512

During each experiment, the progress of the reaction was monitored by Atomic Absorption Spectrometry (AAS) measurements of total iron in solution aliquots taken from the reactor at different leaching times. Also, Eh was measured in the same aliquot with a CORNING Model 340 pH meter. The potential values reported in this work were measured with respect to an Ag/AgCl (3M KCl) electrode, which potential is 0.194 V vs SHE at 25°C.

After completion of each experiment, the pyrite slurries were filtered and washed with distilled water. Then, the solids were dried in stove at 30°C, weighed and stored for SEM-EDX analysis. In the remaining solution of each experiment, iron and copper were analysed by AAS and SO_4^{-2} by precipitation with $BaCl_2$ followed by ultraviolet–visible spectrometry (UV) [21].

3. Results and discussion

3.1. Mineral sample and leaching solutions

XRD diffractogram of the pyrite sample is shown in Figure 1(a) and indicated that contained 99.9% pyrite. Morphological aspects on the surface of a pyrite particle are shown in the SEM micrograph in Figure 1(b). According to EDX analysis, the elemental composition of this particle was 43.8% Fe and 56.2% S (wt. %). Consequently, the molar ratio Fe/S was 0.447, which compares well with the value 0.5 for pyrite with ideal composition.

3.2. Leaching experiments

Results of iron recovery and solution potential vs. time in experiments at different temperatures and different Cu (II) concentrations are presented in Figure 2(a and b), respectively. The curves of iron recovery vs. time show that the iron leaching rate increased with the increase of temperature and Cu (II) concentration in the range studied.

Solution potential curves in these figures show that the average potential established in solution increased with the increase in temperature and Cu (II) concentration, however, the effect was more pronounced in the case of Cu (II) concentration increase. In all cases, the solution potential stabilised after about 10 h of leaching, which indicated that the Cu (II)/Cu (I) ratio in

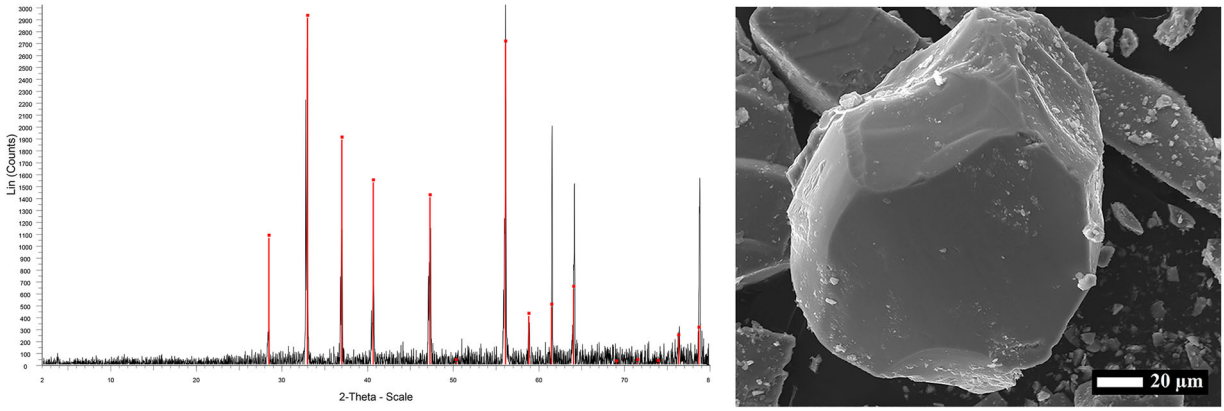

(a) (b)

Figure 1. (a) Diffractogram and (b) SEM micrograph of initial pyrite sample.

solution practically did not change during the experiment. This implies that a stationary stage was reached in which the rate of consumption of Cu (II) by oxidation of pyrite and the rate of formation of Cu (II) by oxidation of Cu (I) by dissolved oxygen became practically equal.

From the values of average potential established in solution in each experiment, the average Cu (II) concentration established in solution was determined by applying Nernst equation. For this purpose, the formal potential $E^{0'}$ was experimentally determined for each experimental condition. Table 2 shows the determined values of formal potential, $E^{0'}$, the average potential established in each experiment, $\bar{E}$, and the calculated average concentration of cupric ion, $\overline{Cu(II)}$. It can be seen that in all experiments the average Cu (II) concentration established in solution was just slightly lower than the initial Cu (II) concentration. This demonstrates that air purging contributed efficiently in each experiment to the regeneration of cupric species in solution.

3.3. Reaction stoichiometry

In solutions with high chloride concentration, Cu (II) and Cu (I) species that predominate are the chloro complexes $CuCl_3^{-1}$ and $CuCl_4^{-3}$, respectively; while, Fe (II) and Fe (III) species that predominate are $FeCl^+$ and $FeCl_2^+$, respectively [10,11]. The chloride leaching of pyrite with Cu (II) can be described in terms of anodic and cathodic sub-processes. The anodic reaction corresponds to pyrite dissolution according to:

$$FeS_2 + 8xH_2O + Cl^- \rightarrow FeCl^+ + (2\text{-}2x)S + 2xSO_4^{-2} + 16xH^+ + (12x + 2)e^- \quad (1)$$

where x represents the fraction of sulphur in the reacted pyrite that is oxidised to sulphate. On the other hand, the cathodic reaction corresponds to

$$CuCl_3^{-1} + Cl^- + e^- \rightarrow CuCl_4^{-3} \quad (2)$$

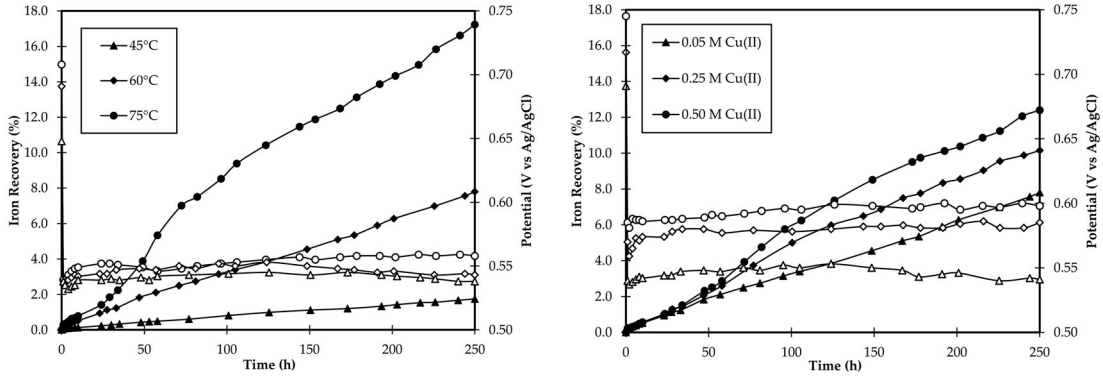

(a) (b)

Figure 2. Evolution of iron recovery and potential vs time (a) at different temperatures and (b) at different Cu (II) concentrations in the leaching of pyrite in cupric chloride solutions.

Table 2. Formal potential, average potential and average Cu (II) concentration established in solution in each leaching experiment.

Exp	$E^{0'}$ (V vs. Ag/AgCl)	$\bar{E}$ (V vs. Ag/AgCl)	$\overline{Cu(II)}$ (mol/L)
A	0.410	0.542	0.0536
B	0.412	0.547	0.0535
C	0.416	0.552	0.0534
D	0.433	0.580	0.2506
E	0.452	0.594	0.5084

Consequently, the general leaching reaction is

$$\begin{aligned} &FeS_2 + (12x+2)CuCl_3^{-1} + 8xH_2O \\ &\quad + (12x+3)Cl^- \\ &\quad \rightarrow FeCl^+ + (12x+2)CuCl_4^{-3} + (2\text{-}2x)S \\ &\qquad + 2xSO_4^{-2} + 16xH^+ \end{aligned} \tag{3}$$

Values of x for each experiment were calculated from the values of iron concentration and sulphate concentration obtained in the leaching solution at the end of the experiment. A summary of the results for each experiment is shown in Table 3. Also, in this table, the fraction of sulphate and sulphur calculated from the reacted pyrite is presented as percentages. Results show that the percentage of sulphate increases from 52% to 62.6% with a temperature increase from 45°C to 75°C. On the other hand, this percentage increases from 54% to 75% with an increase in Cu (II) concentration from 0.0535 to 0.5084 mol/L. The effect of the increase of Cu (II) concentration is by far the most determinant on the increase of sulphate formation, which is presumably related to its effect on increasing the potential established in solution. The observed trend is consistent with previous studies which have shown that the number of electrons involved in the anodic dissolution of a sulphide increases with the applied potential, which was related to an increase in the fraction of sulphur that is oxidised to sulphate ions [22].

3.4. SEM observations on leached pyrite

SEM micrographs in Figure 3 show the surface morphology of leached pyrite particles at the end of each experiment. In every particle, there is presence of holes and cracks, which were not present in the original particles (see Figure 1b), this can be related to the oxidative action of cupric ions during leaching. The observed morphological depressions can be associated to certain sites on the pyrite structure (presumably edges, corners and crystal defects present in the original structure) where pyrite is preferentially oxidised to sulphate ions. The number of holes and cracks formed on the pyrite surface at the end of each experiment increased with the increase in temperature and Cu (II) concentration. This trend is consistent with the percentage of sulphate formation, which also increased with the increase in temperature and Cu (II) concentration, as shown in Table 3.

Table 3. Experimental values of the final concentration of iron and sulphate in solution for each experiment, and calculated values of x and sulphur/sulphate conversion.

Exp	Fe (g/L)	SO_4^{-2} (g/L)	x	S (%)	SO_4^{-2}(%)
A	0.081	0.145	*0.520*	47.98	52.02
B	0.361	0.670	*0.540*	45.99	54.01
C	0.813	1.749	*0.626*	37.42	62.58
D	0.473	1.045	*0.642*	35.78	64.22
E	0.562	1.448	*0.750*	25.03	74.97

The surface morphology obtained in pyrite particles during leaching could be convenient when leaching a pyritic refractory gold ore, as formation of holes and cracks could help to enhance the liberation of occluded gold. From this perspective, operating with a high concentration of cupric ions would be particularly attractive as in this case, the formation of holes and cracks is notably enhanced.

3.5. Reaction kinetics

The kinetics of dissolution of sulphide mineral particles has been generally described according to the shrinking core model (SCM) [23]. There are three main types of control in the SCM, chemical reaction, diffusion through the solid product layer and mixed control, which for spherical particles can be expressed with the following equations, respectively [24]:

$$1 - (1 - X_B)^{\frac{1}{3}} = k_R t \tag{4}$$

$$1 - 3(1 - X_B)^{\frac{2}{3}} + 2(1 - X_B) = k_D t \tag{5}$$

$$\begin{aligned} &\left[1 - 3(1 - X_B)^{\frac{2}{3}} + 2(1 - X_B)\right] \\ &\quad + \frac{k_D}{k_R}\left[1 - (1 - X_B)^{\frac{1}{3}}\right] \\ &\quad = k_D t \end{aligned} \tag{6}$$

where X_B is the fraction of reacted sulphide and k_R, k_D are apparent rate constants. Additionally, k_R and k_D can be expressed as

$$k_R = \frac{bkC_a^n}{\rho R_o} \tag{7}$$

$$k_D = \frac{6bD_eC_a^n}{\rho R_o^2} \tag{8}$$

where b, stoichiometric coefficient; k, intrinsic rate constant (m/h); C_a, oxidising agent concentration (mol/m^3); n, reaction order; ρ, molar density of reacted particle

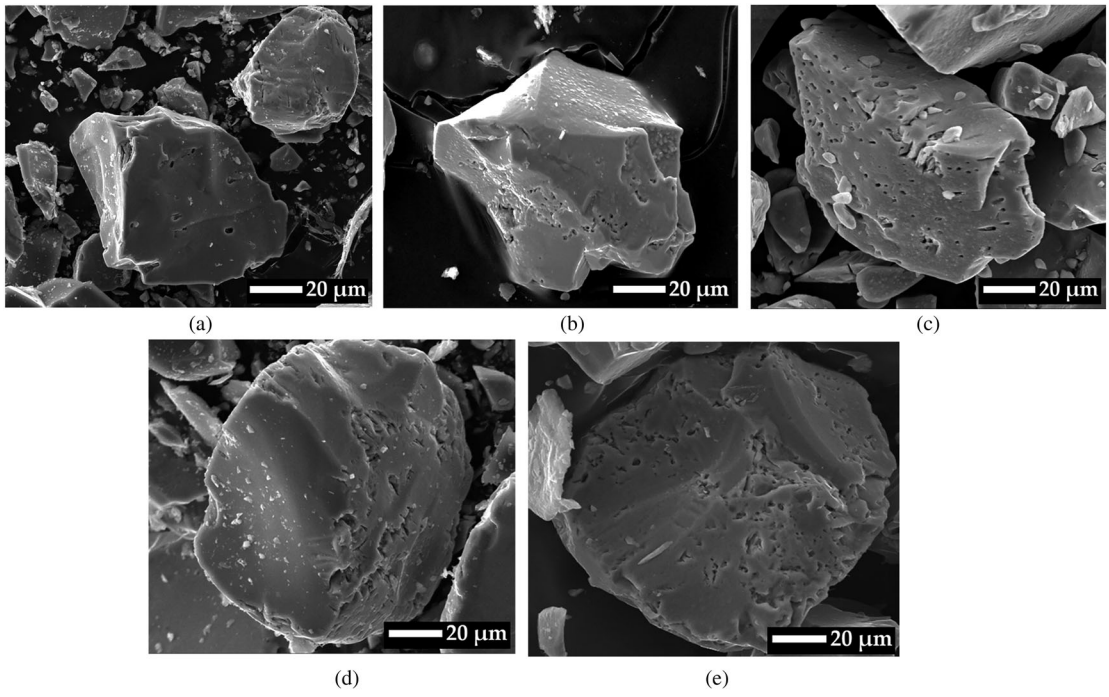

Figure 3. SEM micrographs of the leached pyrite at (a) 0.054 M Cu (II) – 45°C; (b) 0.054 M Cu (II) –60°C; (c) 0.054 M Cu (II) – 75°C; (d) 0.252 M Cu (II) – 60°C and (e) 0.512 M Cu (II) – 60°C.

(mol/m^3); R_o, initial particle radius (m) and D_e, effective diffusivity (m^2/h) [24].

Equations (4)–(6) were tested with the experimental data of iron recovery vs. time from Figure 2(a and b). Figure 4(a and b) show the results of the SCM for the cases which gave the best fitting in each experiment, with correlation coefficients (R^2) higher than 0.99 in all cases. In Figure 4(a), it can be observed that chemical reaction control applies to the 45–60°C range, but then changes to mixed control when temperature was raised to 75°C. In Figure 4(b), it can be observed that chemical reaction control applies to the lowest Cu (II) concentration, 0.054 M, but switches to mixed control at Cu (II) concentrations 0.252 and 0.512 M. The observed change from chemical reaction to mixed control can be associated to the building up of the layer of residual sulphur which introduces at some stage a relevant diffusion controlling process. The appearance of this control can be related to the increase in the degree of pyrite conversion which results in an increase of the thickness of the sulphur layer formed. In fact, data in Table 4 shows that the mixed control was reached only in experiments in which the maximum percentage of dissolved pyrite was over 10%.

Values of the rates constant k_R and k_D determined from the slopes for each experiment are shown in

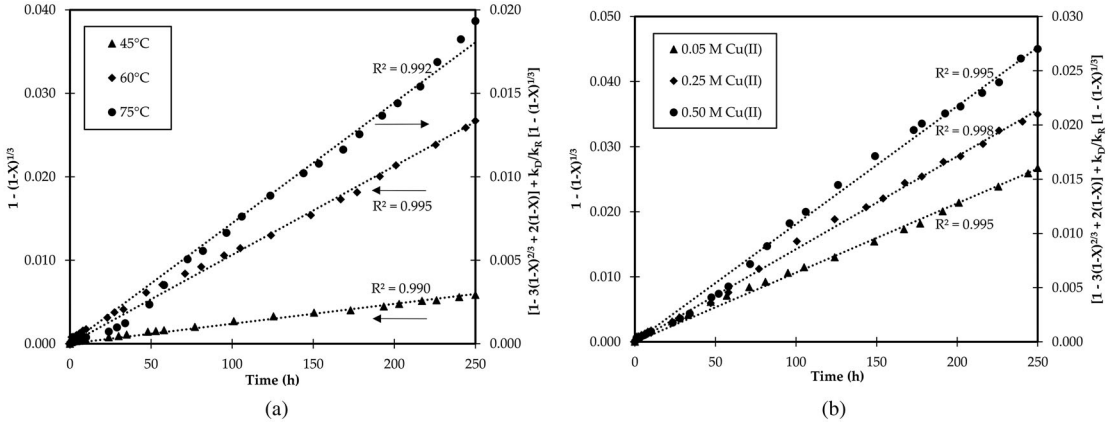

Figure 4. Experimental data plotted according to the Shrinking Core model (a) at different temperatures and (b) at different Cu (II) concentrations.

Table 4. Kinetic parameters in the leaching of pyrite in cupric chloride solutions, according to the Shrinking Core model.

Exp.	X_{FeS_2} (%)	Control	k_R (h^{-1})	k_D (h^{-1})
A	1.75	Chemical reaction	$2.385\ (10)^{-5}$	–
B	7.75	Chemical reaction	$1.064\ (10)^{-4}$	–
C	17.46	Mixed	$2.567\ (10)^{-4}$	$3.612\ (10)^{-5}$
D	10.16	Mixed	$1.473\ (10)^{-4}$	$7.309\ (10)^{-5}$
E	12.07	Mixed	$1.803\ (10)^{-4}$	$9.023\ (10)^{-5}$

Table 4. The activation energy of the leaching of pyrite in cupric chloride solutions was calculated from the Arrhenius plot. The Arrhenius plot was determined by plotting the rate constants, k_R, obtained at different temperatures, as it is shown in Figure 5(a). The activation energy obtained was 73.102 kJ/mol and the pre-exponential term was 2.635×10^7. This activation energy value is in the range of values reported for pyrite dissolution in cupric chloride solutions [9].

For the order dependence of the Cu (II), the rate constant k_R obtained at different Cu (II) concentrations was plotted in logarithmic axes, as it is shown in Figure 5(b). To elaborate Figure 5(b), the average potential established in solution during each leaching experiment was used in order to determine the real Cu (II) concentration (see Table 2). The slope of the line in Figure 5(b) represents the Cu (II) exponent, which had a value of 0.230.

From the previous results, the following kinetic equations were obtained to chemical reaction control (experiments with $T \leq 60°C$ and Cu (II) ≤ 0.054 M) and mixed control (experiments with $T > 60°C$ and Cu (II) > 0.054 M), respectively:

$$1-(1-X_{FeS_2})^{\frac{1}{3}} = 607.304 \cdot \frac{[Cu(II)]^{0.230}}{R_o} \cdot \exp\left(-\frac{8792.676}{T}\right) \cdot t \qquad (9)$$

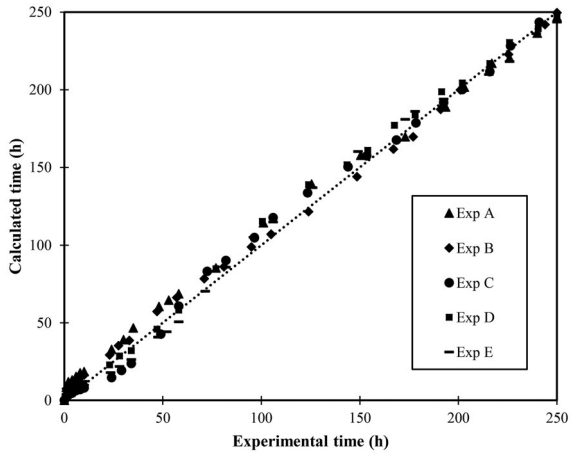

Figure 6. Comparison of experimental and calculated values of leaching time of the pyrite dissolution in cupric chloride solutions.

$$\left[1-3(1-X_{FeS_2})^{\frac{2}{3}}+2(1-X_{FeS_2})\right] + \frac{2.277 \cdot 10^{-16}}{R_o} \cdot \exp\left(\frac{8792.676}{T}\right)\left[1-(1-X_{FeS_2})^{\frac{1}{3}}\right] = 1.383 \cdot 10^{-13} \cdot \frac{[Cu(II)]^{0.230}}{R_o^2} \cdot t \qquad (10)$$

Equation (9) was obtained by combining Equations (4) and (7), while Equation (10) was obtained by combining Equations (6)–(8). In these equations, the k was replaced for Arrhenius equation and n for Cu (II) exponent. The particle radius was placed as a process variable. Figure 6 shows a plot of experimental leaching times versus leaching times calculated with Equations (9) and (10), for all the conducted experiments. In all cases, the models gave an excellent fit with a correlation very

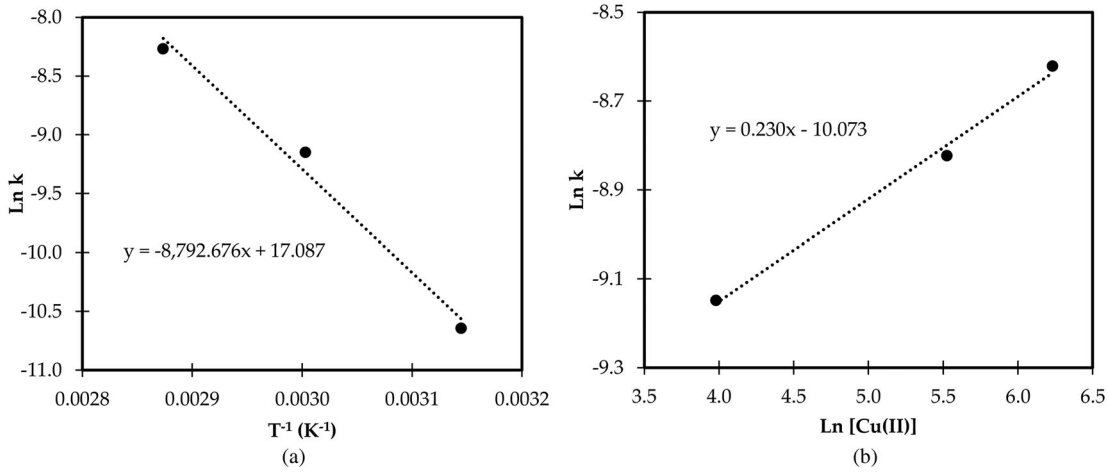

Figure 5. (a) Arrhenius plot and (b) reaction order of Cu (II) for the leaching of pyrite in cupric chloride solutions.

acceptable. Conclusively, Equations (9) and (10) allow to calculate the leaching time (t) to reach a pyrite conversion of interest (X_{FeS_2}) as a function of particle radius (R_o), temperature (T) and Cu (II) concentration for chemical reaction control and mixed control, respectively.

4. Conclusion

- Pyrite dissolution in chloride media with Cu (II) occurs according to the following reaction:

$$FeS_2 + (12x + 2)CuCl_3^{-1} + 8xH_2O + (12x + 3)Cl^- \rightarrow FeCl^+ + (12x + 2)CuCl_4^{-3} + (2\text{-}2x)S + 2xSO_4^{-2} + 16xH^+$$

Values of x are related to the fraction of sulphur present in dissolved pyrite which is oxidised to sulphate. Values of x increase in the range 0.520–0.626 with an increase of temperature in the range 45–75°C, and in the range 0.540–0.750 with an increase of Cu (II) concentration in the range 0.0535–0.5084 M.

- Oxidation of pyrite to sulphate shows in the formation of holes and cracks on the surface of leached pyrite particles, which also increase with an increase in temperature and Cu (II) concentration.
- The kinetics of cupric leaching of pyrite in chloride solutions can be described by the shrinking core model with chemical reaction control ($T \leq 60$°C and Cu (II) ≤ 0.054 M) or mixed control ($T > 60$°C and Cu (II) > 0.054 M), according to the equations:

$$1 - (1 - X_{FeS_2})^{\frac{1}{3}} = 607.304 \cdot \frac{[Cu(II)]^{0.230}}{R_o} \cdot \exp\left(-\frac{8792.676}{T}\right) \cdot t$$

$$\left[1 - 3(1 - X_{FeS_2})^{\frac{2}{3}} + 2(1 - X_{FeS_2})\right] + \frac{2.277 \cdot 10^{-16}}{R_o} \cdot \exp\left(\frac{8792.676}{T}\right)\left[1 - (1 - X_{FeS_2})^{\frac{1}{3}}\right] = 1.383 \cdot 10^{-13} \cdot \frac{[Cu(II)]^{0.230}}{R_o^2} \cdot t$$

Acknowledgements

The authors thank CONICYT Basal Project FB0809 (AMTC) in funding this work and SENESCYT in supporting K. Jaramillo studies.

Disclosure statement

No potential conflict of interest was reported by the authors

Funding

This work was supported by CONICYT Basal Project FB0809 (AMTC).; Comisión Nacional de Investigación Científica y Tecnológica

ORCID

Katherine Jaramillo http://orcid.org/0000-0002-6856-6428
Tomás Vargas http://orcid.org/0000-0002-4144-2329

References

[1] Chandra AP, Gerson AR. The mechanisms of pyrite oxidation and leaching: a fundamental perspective. Surf Sci Rep. 2010;65(9):293–315.
[2] Bryson LJ, Crundwell FK. The anodic dissolution of pyrite (FeS2) in hydrochloric acid solutions. Hydrometallurgy. 2014;143:42–53.
[3] Fraser KS, Walton RH, Wells JA. Processing of refractory gold ores. Miner Eng. 1991;4(7):1029–1041.
[4] La Brooy SR, Linge HG, Walker GS. Review of gold extraction from ores. Miner Eng. 1994;7(10):1213–1241.
[5] Fernández RR, Sohn HY, LeVier KM. Process for treating refractory gold ores by roasting under oxidizing conditions. Min Metall Explorat. 2000;17(1):1–6.
[6] Thomas KG. Alkaline and acidic autoclaving of refractory gold ores. JOM. 1991;43(2):16–19.
[7] Lynn NS. The bioleaching and processing of refractory gold ore. JOM. 1997;49(4):24–26.
[8] Lampinen M, Seisko S, Forsström O, et al. Mechanism and kinetics of gold leaching by cupric chloride. Hydrometallurgy. 2017;169:103–111.
[9] Elomaa H, Rintala L, Aromaa J, et al. Open circuit potential and leaching rate of pyrite in cupric chloride solution. Can Metall Q. 2018;57(4):416–421.
[10] Winand R. Chloride hydrometallurgy. Hydrometallurgy. 1991;27(3):285–316.
[11] Havlík T. Chapter 8 - Leaching in chloride media. In: Havlík T, editor. Hydrometallurgy: Principles and Applications. Cambridge, England: Cambridge International Science Publishing Ltd and Woodhead Publishing Ltd; 2008. p. 242–254.
[12] Lundström M, Aromaa J, Forsén O. Redox potential characteristics of cupric chloride solutions. Hydrometallurgy. 2009;95(3):285–289.
[13] Hyvärinen O, Hämäläinen M, Lamberg P, et al. Recovering gold from copper concentrate via the HydroCopper™ process. JOM. 2004;56(8):57–59.
[14] Yazici EY, Deveci H. Extraction of metals from waste printed circuit boards (WPCBs) in H_2SO_4–$CuSO_4$–NaCl solutions. Hydrometallurgy. 2013;139:30–38.
[15] McDonald GW, Saud A, Barger MS, et al. The fate of gold in cupric chloride hydrometallurgy. Hydrometallurgy. 1987;18(3):321–336.

[16] Nicol MJ, Zhang S. Anodic oxidation of iron(II) and copper(I) on various sulfide minerals in chloride solutions. Hydrometallurgy. 2016;166:167–173.
[17] Nicol MJ, Tjandrawan V, Zhang S. Cathodic reduction of iron(III) and copper(II) on various sulfide minerals in chloride solutions. Hydrometallurgy. 2016;166:113–122.
[18] Nicol M, Zhang S, Tjandrawan V. The electrochemistry of pyrite in chloride solutions. Hydrometallurgy. 2018;178:116–123.
[19] Elomaa H. Leaching of pyrite in cupric chloride media. Espoo, Finland: Aalto University; 2016.
[20] Parthasarathy H, Baltrus JP, Dzombak DA, et al. A method for preparation and cleaning of uniformly sized arsenopyrite particles. Geochem Trans. 2014;15(1):14–20.
[21] Franson M, Greenberg A, Eaton A, et al. 4500-SO4 2-sulfate: standard methods for the examination of water and wastewater. 20th ed Washington (DC): American Public Health Association; 1998.
[22] Jordan H, Vargas T. Modeling the kinetics of anodic dissolution of chalcopyrite based on electrochemical measurements conducted on chalcopyrite particle electrodes. ECS Trans. 2010;28(6):201–209.
[23] Wadsworth ME, Miller JD. Hydrometallurgical processes. In: HY Sohn, ME Wadsworth, editor. Rate processes of extractive metallurgy. Boston, MA: Springer US; 1979. p. 133–244.
[24] Habashi F. Kinetics of metallurgical processes. Québec, Canada: Métallurgie Extractive Québec; 1999.